CRINC

(NASA-CR-173452) NUMERICAL ANALYSIS OF A VARIABLE CAMBER ROTOR BLADE AS A LIFT CONTROL DEVICE Final Report (NASA) 50 p HC A03/MF A01 CSCL 01C

N84-21538

Unclas G3/05 18975

THE UNIVERSITY of KANSAS CENTER FOR RESEARCH, INC.

2291 Irving Hill Drive-Campus West Lawrence, Kansas 66045

Final Report
for
NASA Cooperative Agreement
NCC2-92

"INVESTIGATION OF VARIABLE CAMBER DEVICES FOR
HELICOPTER ROTOR SYSTEMS

NUMERICAL ANALYSIS OF A VARIABLE CAMBER ROTOR BLADE AS A LIFT CONTROL DEVICE

by

Alfred O. Awani

Flight Research Laboratory
University of Kansas Center for Research, Inc.
Lawrence, Kansas 66045

April 1984

NUMERICAL ANALYSIS OF A VARIABLE CAMBER ROTOR BLADE AS A LIFT CONTROL DEVICE

Alfred O. Awani
Research Associate
University of Kansas
Lawrence, Kansas 66045

and

Robert H. Stroub
Aerospace Engineer
NASA Ames Research Center
Moffett Field, California 94035

ABSTRACT

A new rotor configuration called the variable camber rotor was numerically investigated as a lift control device. This rotor differs from a conventional (baseline) rotor only in the blade aft section. In this configuration, the aft section or flap is attached to the forward section by pin joint arrangement, and it is also connected to the rotor control system for the control of rotor thrust level and vectoring. It is pilot action to the flap deflection that controls rotor lift and tip path plane tilt. This report presents the drag due to flaps and correlate the theoretical result with test data. The assessment of payoff for the variable camber rotor in comparison with conventional (baseline) rotor was examined in hover. The variable camber rotor is shown to increase hover power required by 1.35%, but such a minimal power penalty is not significant enough to be considered

a negative result. In forward flight, the control needs of the variable camber rotor was evaluated. The result of the evaluation indicated that the variable camber rotor requires a flap setting of $\delta_{f90} = -8.198°$ and $\delta_{f270} = 29.998°$ respectively. However, the excessive negative flap deflection at the advancing blade region makes it impractical for use as a lift control device because it failed to demonstrate the ability to decrease rotor power requirements and resulted in reduced cruise efficiency.

NOMENCLATURE

A_0	Collective pitch, deg
A_{1s}, B_{1s}	Coefficients in the representation of rotor-blade cyclic pitch that is $\theta_c = -A_{1s} \cos \psi - B_{1s} \sin \psi$, deg
b	Number of blades
c	Blade or airfoil chord
c_d	Blade element drag coefficient, drag/qc
C_ℓ	Blade element lift coefficient, Lift/qc
$C_{\ell_\delta} = \frac{\partial C_\ell}{\partial \delta}$	Variation of sectional lift coefficient with control surface deflection, deg^{-1} or rad^{-1}
$C_{h_\delta} = \frac{\partial C_h}{\partial \delta}$	Variation of hinge moment coefficient with control surface deflection, deg^{-1} or rad^{-1}
$C_{h_\alpha} = \frac{\partial C_h}{\partial \delta}$	Variation of hinge moment coefficient with angle of attack, deg^{-1} or rad^{-1}
C_T/σ	Rotor thrust coefficient (shaft-axes lift coefficient) thrust/ $\rho S(\Omega R)^2$
L/D_e	Lift/drag ratio
M	Mach number
M(1)(90)	Rotor-blade tip Mach number at 90° azimuth position
M(1)(270)	Rotor-blade tip Mach number at 270° azimuth position
q	Dynamic pressure, 1/2 ρV^2
q_1	Bending displacement, m
R	Blade radius, m
S	Reference area [(number of blade) x (blade chord) x (rotor radius)]
V	Free stream velocity, knots

NOMENCLATURE (continued)

μ	Advance ratio, V/ ΩR
α	Blade element angle of attack, deg
α_c	Angle of attack of control axis (swashplate) positive tilted aft, deg
α_s	Angle of rotor shaft from vertical, positive shaft tilted aft, deg
β	Flapping response, deg
δ_f	Flap deflection, deg
δ_0	Steady component of flap deflection, deg
δ_{nc}	cos n ψ component of flap deflection, deg
δ_{ns}	sin n ψ component of flap deflection, deg
ζ	lag angle, deg
ϕ	Inflow angle of attack, deg
θ	Blade section pitch angle measured from the reference plane to the zero-lift line.
θ_c	cyclic pitch, deg
$\theta_{.75}$	Collective pitch at 0.75R, deg
ρ	Density of air, kg/m^3
σ	Rotor Solidity, bc/ π R
ν	Induced inflow velocity, m/sec
ψ	Rotor-blade azimuth angle, deg
Ω	Rotor speed, rad/sec
ΩR	Rotor tip speed, m/sec

INTRODUCTION

Two problems constrain the flight capability of conventional helicopters. The first is available power and the second rotor systems loads. Aerodynamic efficiency of fixed geometry blades inevitably decreases in high speed as regions of the rotor disc become disproportionally loaded. Rotor and control system loads build up as a direct result of increasingly severe advancing blade compressibility effects combined with the retreating blade stall effects. In seeking to relieve the various forward-flight limitations and maintain good hover performance, a rotor utilizing variable camber was conceived as a lift control device that could significantly reduce control loads and eventually reduce total rotor system vibratory loads.

The variable camber design that is the subject of this report incorporates a large chord trailing edge flap for blade lift control to reduce control loads and improve performance, while keeping the rotor control system as simple as possible. By using large chord flap, rotor lift control would be effected with small flap deflection, and so with small drag penalties and pitching moment excursions. With lift control being accomplished by flaps, then control loads could be greatly reduced through structural attachment of the flap to the blade combined with aerodynamic balances. Reference 1 presents data on application of flap balance techniques to variable camber rotors and it was found that all the techniques were effective in reducing hinge moment.

This report expands the initial investigation (Reference 1) of the variable camber rotor concept by correlating the theoretical results of the drag due to flaps with test data, and also evaluates the control needs of the concept in forward flight.

DESCRIPTION OF VARIABLE CAMBER CONCEPT

Figures 1 and 2 shows the variable camber rotor with the flap neutral and the flap deflected respectively, and also delineates other features of the concept that are vital to achieving the design objectives. The primary features and their functions are as follows:

- The primary load carrying structure is the forward section of the blade and is not connected to the control system.
- The forward section is fixed. The flap is used for lift modulator and rotor tilt.
- The forward section has mechanical properties that are stiffer than the aft section (trailing edge flap) in all directions.
- The aft section or trailing edge flap is attached to the forward section by a pin joint arrangement. It is also connected to the control system such as a swashplate for the control of rotor thrust level and vectoring. This section is configured by aerodynamic and mechanical techniques to achieve low flap hinge moments.
- The rotor hub is a conventional articulated hub or hingeless.

In view of the fact that the primary load carrying structure is the forward section of the blade; and is not connected to the control system, the benefit of control by deflection of the flap should present an economical system for attaining the control forces and moments, since the control system (trailing edge flap) react only a small amount of loads generated by the blade; hence its potential for having high loads is greatly reduced by the design concept itself.

There is one area of concern that could affect the viability of the concept. The drag of flapped configuration being more than that for conventional rotor. The drag due to flap deflection will first be reviewed.

DRAG DUE TO FLAPS

Having decided in Reference 1 that the trailing edge flaps were the best choice for variable camber concept, a preliminary configuration was adopted which included a plain flap with 0.50 chord ratio (see Figure 3). The 0.50 chord ratio was selected because of its potential for providing relatively high maximum lift coefficient (in the 1.6 - 1.9 range), but mainly because of the large ΔC_L per degree of flap deflection. This latter characteristic enables the use of small deflections to obtain the desired lift hence, they minimize the drag increment involved.

Theoretical method -: The two dimensional characteristics of the flapped airfoils were evaluated by means of two airfoil analysis methods.

1. The viscous transonic analysis (reference 2).
2. The viscous/potential flow past single-element and multielement airfoils (Reference 3).

The theoretical method of Reference 2 (Program H.) consists of the analysis of transonic flow past a supersonic wing section, which includes the effect of a boundary layer correction. This method computes the transonic flow with shock waves around a given airfoil at a prescribed Mach number and angle of attack. The program consist of two parts. The first part process the airfoil coordinates and does a conformal mapping onto the unit circle, while the second part solves the transonic flow equations for a specified Mach number and angle of attack. The first part need only be executed once, and then the second part can be repeated for various Mach numbers and angle of attack. The boundary layer correction is added to restore the original shape of the airfoil if there is no separation. The method of reference 2 furnishes a physically adequate computer simulation of the compressible flows that arise in practical problems of transonic aerodynamics.

The theoretical method of Reference 3 consists of iteratively coupled potential flow, boundary layer, and viscous-wake analyses. With the exception of a compressibility correction in the potential-flow calculation, the analysis assumes that the effects of compressibility are negligible. While in the case of the viscous flow analysis, the viscous calculations are separated into three types of flows: conventional boundary layers, turbulent

wakes, and confluent boundary layers. The first step in obtaining a complete viscous calculation is the analysis of the conventional boundary layer on upper and lower surfaces of the main airfoil. These upper-surface and lower surface boundary-layer calculations provide the conditions for initializing the turbulent wake analysis at the trailing edge of the main component. These analyses included Mach number and Reynolds number characteristics as a function of angle of attack. The Mach number and Reynolds number ranges were established based on the rotor environment in forward flight (see Reference 4, figures 2 and 3).

Test/Theory Correlation -: In order to validate the drag values determined for the flapped airfoils, using theoretical analysis, the performance measured in the wind-tunnel test of Reference 5 for a NACA 65-210 airfoil with a 50-percent-chord flap was compared to the performance estimated for similar configuration using the airfoil code of Reference 2. The analysis found that fairly satisfactory agreement between test and theory were obtained (see Figures 4 to 5).

Figure 5 shows the drag curves for the NACA 65-210 airfoil section. From figure 5, it was observed that the highest lift coefficient for which a low drag coefficient was obtained was 0.80 for a flap deflection of 10 degrees. The corresponding drag coefficient, 0.0059, was much less than that of the plain airfoil at the same lift coefficient. The lift coefficients data are presented in figures 6 and 7.

The lift, drag and pitching moment characteristics of the unflapped airfoils were also determined by the same airfoil analysis codes to afford direct comparative data. The lift, drag and pitching moment coefficients (taken from Reference 1) are presented in Figures 8 to 10.

Though the lift, drag and pitching moments coefficients values generated by the airfoil analysis methods are considered reasonable, the magnitude of the increment in drag coefficient was compared by plotting the lift coefficient versus drag coefficient for a VR-7 airfoil with 0.50c flap deflected 10 degrees given in figure 9. Figure 9 shows that the highest lift coefficient for which a low drag was obtained by theoretical analysis was 0.79 for a flap deflection of 10 degrees. The corresponding drag coefficient, 0.0059 was less than that of the unflapped VR-7 airfoil with a drag coefficient of 0.007 at the same lift coefficient of 0.79. This tends to correlate well with the values obtained by experimental analysis for the NACA 65-210 airfoil for a flap deflection of 10 degrees (see Reference 5).

Also, presented (in figure 11) are the theoretical results of the lift/drag polars for the NASA A-1 airfoil with 35 percent and 50 percent trailing edge chord flap ratios respectively, obtained from Reference 6. Figure 11 shows that the positive lift coefficient range for which a low drag was obtained for $C_{f/c}$ = 0.50 and $C_{f/c}$ = 0.35 respectively, as compared with the unflapped airfoil was C_ℓ = 0.6 to 1.6. However, there was no clear ceiling values for ΔC_d, but it was clear from figure 11 that the drag coefficient of 0.0208 at C_ℓ = 1.6 for $C_{f/c}$ = 0.50 was much less than the drag coefficient of 0.023 for $C_{f/c}$ = 0.35 at the same lift coefficient. It was also observed from the data presented in figure 11 and in Reference 5 that the range of C_L where the drag is low for an airfoil with a large chord flap could be shifted to a higher lift coefficients with small flap deflections. It is obvious therefore, that it should be possible to use a flap of this type to maintain low profile drags through a wide range of lift coefficient.

Another interesting characteristic shown by the lift/drag polars (see figure 12), is the difference in growth of the drag between the positive and negative lift ranges for the unflapped airfoil and the flapped airfoils. Since a rotor blade is likely to encounter negative lift levels only at high subsonic Mach numbers (i.e. advancing blade), care must be exercised in defining the lower branch of the drag polars at Mach numbers above 0.6, for rotor blades with positive flap deflections.

In general, empirical adjustments between test and theory seems to be very small (see figures 4 to 7), and would not contribute to the validity of the assessment of the usefulness of variable camber concept.

HOVERING ROTOR PERFORMANCE

To evaluate the hover performance characteristics of a rotor blade equipped with a 0.50 chord flap as described above, a prescribed wake hover computer program called PWAKE was used (Reference 7). The PWAKE is based on the application of lifting line theory to the calculation of rotor hover performance, with a prescribed wake representation derived from experimental flow visualization studies of model rotor wakes. The PWAKE program required that thrust coefficient and collective pitch be input; the program takes the collective pitch and iterates on it to obtain the desired thrust coefficient. The program was run first with the flapped rotor blade at values of $C_{T/\sigma}$ of 0.06, 0.078 and 0.09, a range which covers most of the hover regime of helicopters; and then again with a rotor with the unflapped airfoil, for a direct evaluation of the effect of flaps are made.

The program input was arranged such that the model rotor blade was configured as follows: the aft section as measured from $C_{f/c} = 0.50$ has a constant 2 degrees flap deflection from the roof cutout to the tip. The airfoil section used is a NASA A-1 from root cutout to the tip. Both the flapped and the unflapped rotor blades has 8 degrees of linear geometric twist. The section aerodynamic characteristics required are the static lift and drag coefficients as a function of angle of attack and Mach number: $C_L(\alpha,M)$ and $C_d(\alpha, M)$.

The principle overall results is shown in figure 13, a plot of power coefficient for various thrust conditions. Figure 13 shows that there is a very small power penalty for the flapped rotor as compared with the unflapped case. Figure 14b shows the curve representing the induced torque for that case; it is apparent from the plots that the induced torques show a minimal decrement from 0.91R station to the tip with the flap deflected rather than with it retracted. This can be attributed to the small change in lift distribution experienced in the same area (see figure 14a). The profile power distribution is displayed in Figure 14c. It is apparent from figure 14c that the profile power loading show a minimal increment from 0.375R station to the tip with the flap deflect rather than with it retracted.

The total power breakdown is as follows for the case of $C_{T/\sigma} = 0.08$ and $\theta_{.75} = 6.39$

	Profile Power (HP)	Induced Power (HP)	Total Power (HP)
Unflapped rotor	278.5	984.3	1262.8
Flapped rotor (δf=2°)	300.8	979	1279.8
ΔHP due to flaps	+22.3	-5.3	+17

Thus, there is a penalty of 22.3 hp in profile power and an improvement 5.3 hp in induced power giving a total power penalty of 17 hp or 1.35% over the unflapped case. Such a minimal power penalty is not significant enough to be considered a negative result. However, the present configuration does not establish the need for variable camber concept in hover.

THE MATH MODEL FOR FORWARD FLIGHT

To examine the potential of the variable camber rotor in forward flight, an existing state of the art math model was modified to represent the variable camber rotor (see Reference 8). The basis for the math model is a model of the wake trailed by each blade, represented by groups of straight vortex segments with linearly varying vorticity from one end to the other of each segment. This representation included the following modeling features:

1. Blade elastic properties are represented by a modal approach.

2. Aerodynamic formulation is based on a lifting line system, which includes an approximation of unsteady aerodynamic effects, dynamic stall delay, radial flow, reverse flow and three dimensional tip relief effects.

3. The vortex sheet trailed by each blade is modeled by a system of vortices identified as the near-wake, attached to the blade quarter chord line and trailed 1/24th of a revolution ($\Delta\psi = 15°$) and a midwake, which extends for two additional time intervals ($\Delta\psi = 30°$) beyond the near wake.

4. The rotor blade is subdivided into 13 spanwise segment of equal length, from root cutout to tip, thus the vortex sheet trailed by each blade is represented by 13 horseshoe vortices. Except for the initial "Betz" rollup criteria which set the spanwise location of the tip vortices, the wake model is otherwise rigid, and its displacement is a combination of flight kinematics with a uniform induced downwash velocity.

To simplify the modeling of the variable camber distributions, provisions have been made to prescribe independent variable camber levels for each of the 13 blade panels. At each computational panel, the trailing edge flap deflection around the azimuth can be prescribed as a Fourier series consisting of a steady value and up to two harmonics as shown below:

$$\delta_F(\psi) = \delta_0 + \sum_{n=1}^{2} (\delta_{nc} \cos n\psi + \delta_{ns} \sin n\psi)$$

The benefit of this approach is that while the current wake model cannot account for any of the secondary roll up of the vortex sheet due to highly localized lift variations, each computation panel will carry its own horseshoe vortex for $\Delta\psi = 45°$ (i.e. 1/8 of a revolution).

The unsteady and radial flow corrections are a simplication of the model described in Reference 9. Transonic 3-D relief corrections for the drag coefficient were introduced following the procedure outlined in References 10 and 11. Tip relief on pitching moments is carried out by relieving the 2-D data at Mach numbers beyond M = 0.7 by AR = 1.0 trends.

The most significant limitations of this or any math model that affects the applicability of the variable camber concept is the unsteady aerodynamics effects which remain somewhat uncertain. However, since the objective herein is to investigate variable-camber rotor configuration and not to investigate methodology, the present formulation modeled all unsteady aerodynamics effects on the basis of data from 2-D airfoils undergoing some form of sinusoidal motion (pitching) at constant Mach number. Also it should be noted that in the variable camber rotor there are contributions to the shed vorticity from camber changes (e.g. flap motions) which are only in part accounted for by the current formulation, since camber variation introduces effects not described by the fixed relationship between angle of attack and lift.

CONTROL NEEDS IN FORWARD FLIGHT

The present variable camber design concept utilizes a single control input with a unique combination of collective and cyclic flap deflection values to generate the same trim condition, as the baseline (conventional rotor) case.

Variable-camber control devices as suggested herein, obviously imply the control by deflection of the blade trailing edge flaps. As indicated in the section on (The Math Model For Forward Flight), the flap deflection schedules were defined by the following equations:

$$\delta_F(\psi) = \delta_0 + \sum_{n=2}^{2} (\delta_{nc} \cos n\psi + \delta_{ns} \sin n\psi)$$

For the variable camber concept the range of collective and lateral flap inputs were limited to +10.9 and -1.4 degrees respectively. This selection was based on previous work on variable camber rotor. The initially selected value for the harmonic sine of -15.5 degrees was extended to include both the -17.5 and the -19.098 degrees region, when early trend indicated the need for additional longitudinal cyclic control. The cyclic inputs were restricted to limit the maximum resultant or allowable flap deflection based on the stacking or combining of the collective flap input and the harmonics to δ_{f270} = 30 degrees.

These collective and first harmonic flap inputs were felt to bracket the probable range of acceptable flap travel to trim. With the boundaries of flap deflection established by the models, the next step is to determine the degree of correlation between the models and the actual trim. This is achieved by running additional selective cases and using the results for comparison and to upgrade the model. Thus, trim control therefore became of problem of selecting the control combinations that result in the most favorable trade-off of performance parameter.

The computed values for the final flap deflections required for a given flight condition are presented in Table 1. The results presented in Table 1 indicated that the rotor blade requires a final flap deflection of -8.198 degrees at the advancing blade 90 degrees azimuth position; and 29.998 degrees at the retreating blade 270 degrees azimuthal position.

TABLE 1. FINAL FLAP DEFLECTIONS

ADVANCE RATIO $= \frac{V}{\Omega R}$	VELOCITY V KNOTS	ROTOR BLADE TIP MACH NUMBER AT 90° AZIMUTH POSITION M (1)(90)	ROTOR BLADE TIP MACH NUMBER AT 270° AZIMUTH POSITION M (1)(90)	FLAP DEFLECTION AT 90° AZIMUTH POSITION δ_{f90}, DEG	FLAP DEFLECTION AT 270° AZIMUTH POSITION δ_{f270}, DEG
0.50	192.3	0.85	0.284	-8.198	29.998

CRUISE PERFORMANCE COMPARISON

The effect of the variable camber concept on cruise performance was evaluated by a side-by-side comparison between the baseline (conventional) rotor and the variable camber rotor with low propulsive requirements. It is shown below that the variable camber rotor required more power than the baseline rotor at 192 knots (see Figure 15). The higher power requirements in terms of reduced cruise efficiency is shown below:

	BASELINE ROTOR	VARIABLE CAMBER ROTOR
L/DE	10.3	4.86
FH	2.581	2.753
$\overline{X}$	.014	.014
HP	824.943	1580

where the variable camber concept incurred cruise L/D_e reduction of 48% at 192 knots. Compared to the baseline rotor of identical flight condition, the variable camber concept utilizing the present design features failed to demonstrate the ability to decrease rotor power requirements in forward flight and markedly reduced cruise efficiency.

The reduced efficiency of the variable camber rotor accrues from two basic phenomena. First, the negative flap deflection in the critical region around $\psi = 90°$, increased the shaft driving power through higher drag coefficients on the advancing portion of the blade. This higher drag could in turn increase the high transonic drag in this area. Second, the excessive flap deflections required at the retreating portion of the blade and at particular

azimuthal locations, does negate the benefit of the variable camber concept as a lift control device. This is depicted in figure 16, where the variable camber rotor increased the shaft driving power through the higher drag coefficients at ψ = 43° to 360°. This is further substantiated in figure 17 for ψ = 90°, where the drag is greatly increased around the tip region for the variable camber rotor. Figure 18 shows that the variable camber rotor resulted in change in the azimuthal lift distribution. The primary difference between the two rotor configurations are the oscillatory peak values of the lift. At 192 knots the variable camber rotor generated 863N more lift than the baseline rotor. It is seen that the variable camber rotor does experience more negative lift, and the corresponding high drag coefficients in the critical region around ψ = 90°. Thus, the variable camber concept is seen to increase power requirements by carrying more negative lift on the usual negative lift region on the advancing portion of the disk. This in turn, increase the high transonic drag in this area (see figure 19). Also from figure 20, it can be seen from the curves of the rotor horsepower that the variable camber rotor shows a power increment at ψ = 77° to 293°. This is further substantiated in figure 21, which shows that the variable camber rotor increased the rotor power requirements at ψ =0° to 17° and at ψ = 68° to 345°. From figure 21, it could be inferred that the variable camber rotor will increase shaft driving power with an increase in flap deflection.

In the above discussion, it was pointed out that the variable camber rotor generate more lift, than the baseline configuration. This characteristics is inherent to the variable camber concept and occurs with the pilot action to the flap deflection to control rotor lift and tip path plane tilt.

While, in principle, the changes in maximum lift coefficient cannot be separated from the pitching moment coefficient changes, the relatively large blade pitching moment coefficient as depicted in figure 22 did result in large negative (nose-down) moment coefficient at ψ = 0° to 32° and at ψ = 142° to 345°. Also at ψ = 32° to 137°, the variable camber rotor did experience a nose-up pitching moment coefficient due to the negative flap deflection in the advancing blade region. Figure 23 show further detail of this effect.

Another mechanism by which the variable camber rotor increased the need for a very torsionally stiff blade was by defining a sinusoidal flap deployment schedule that increases the blade elastic twist. This was achieved by a systematic variation of flap deflection angle around the azimuth. The increase in elastic twist could be attributed to the relatively large blade pitching moment coefficient (see figure 22), which had an adverse effect on rotor performance because of change in effective twist due to torsion on the blade (see figure 24). With a view to decreasing or eliminating the elastic torsional deflections of the variable camber rotor blade, the present variable camber design concept accepted a rigid blade by increasing the torsional frequency of the blade.

As indicated above, the configuration analyzed herein does not show an improvement in rotor cruise performance, however, other factors need to be kept in mind which could affect this result. The deflection of the flap at the tip region, region of high Mach number is not considered viable, since the flap deflection resulted in high rotor power consumption. One method to avoid this situation would be to use the flap only at any portion of the

blade inboard of 0.90R, and use another device like the free-tip rotor discussed in Reference 12 to handle the tip region.

SUMMARY AND CONCLUSIONS

The results of this study have shown that analytically the variable camber rotor failed to demonstrate the ability to decrease rotor power requirements in forward flight and markedly reduced cruise efficiency. The reduced efficiency was the result of excessive flap deflections at particular azimuthal locations, which makes it impractical for use as a lift control device.

The test/theory correlation for drag due to flaps shows very good agreement at all but few conditions. It was shown that large chord flaps are desirable, since they minimize the drag increment involved. Also, it was observed from the data presented, that the range of C_L where the drag is lower for an airfoil with large chord flap could be shifted to higher lift coefficients with small flap deflections. Thus, it is obvious that it should be possible to use a flap of this type to maintain low profile drag through a wide range of lift coefficients.

The hovering rotor performance shows a minimal power penalty of 1.35% for the variable camber rotor over the unflapped case, this power penalty is not significant enough to be considered a negative result. However, the present configuration does not establish the need for variable camber concept in hover.

The results presented herein are from math models with known limitations that are applicable to the baseline (conventional) rotor configuration as well as applicable to the variable camber rotor.

RECOMMENDATION

The variable camber rotor (trailing edge flap) should be used only at any portion of the blade inboard of 0.90R, another device should be used to handle the tip region.

REFERENCES

1. Awani, Alfred O.: The Investigation of a Variable Camber Blade Lift Control for Helicopter Rotor System, NASA CR 3503, January 1982.

2. Bauer, Frances; Garabedian, Paul; Korn, David: and Jameson, Anthony: Supercritical Wing Sections II, Lecture Notes in Economic and Mathematical Systems, Vol. 108, Springer-Verlag, 1975.

3. Olson, L.E.; James, W.D.; and McGown, P.R.: Theoretical and Experimental Study of the Drag of Single and Multielement Airfoils. J. Aircraft, Vol. 16, No. 7, July 1979.

4. Awani, Alfred O.: Doctor of Engineering Project Proposal for the Analysis of a Variable Camber Rotor. University of Kansas, Lawrence, Kansas, KU-CRINC-480-1, September 1980.

5. Klein, Milton M.: Pressure Distributions and Force Tests of an NACA 65-210 Airfoil Section With A 50-Percent Chord Flap. NACA TN 1167, January 1947.

6. Dadone, L.; Cowan, J.; and McHugh, F.J: Variable Camber Rotor Study, NASA CR 166382, August 1982.

7. Landgrebe, Anton J.: An Analytical and Experimental Investigation of Helicopter Rotor Hover Performance and Wake Geometry Characteristics, USAAMRDL TR 71-24, June 1971.

REFERENCES (CONT.)

8. Sewell, R.; Lee, S.; and Fukushima, T.: Rotor Airloads and Performance Analysis with Non-Uniform Induced Inflow. Boeing Document D8-0312, December 1967.

9. Gormont, R.E.: A Mathematical Model of Unsteady Aerodynamics and Radial Flow for Application to Helicopter Rotors; USAAMRDL TR 72-67, May 1973.

10. Lenard, John M.; Boehler, G.D.: Inclusion of Tip Relief in the Prediction of Compressibility Effects on Helicopter Rotor Performance, USAAMRDL TR 73-71, December 1973.

11. Lenard, J.M.: A Theoretical Analysis of the Tip Relief Effect on Helicopter Rotor Performance, USAAMRDL TR 72-7, August 1972.

12. Stroub, Robert H.: An Analytical Investigation of the Free-Tip Rotor for Helicopters. NASA TM 81345.

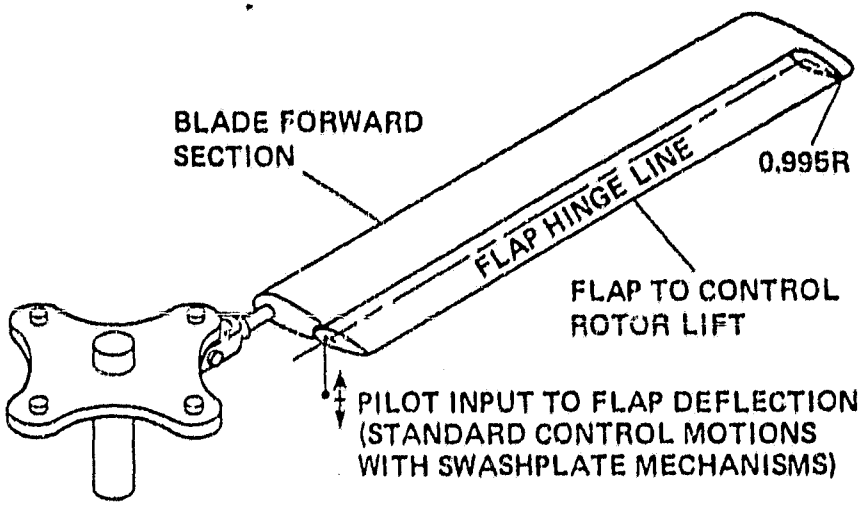

Figure 1. Variable Camber Rotor Blade With Flap Neutral

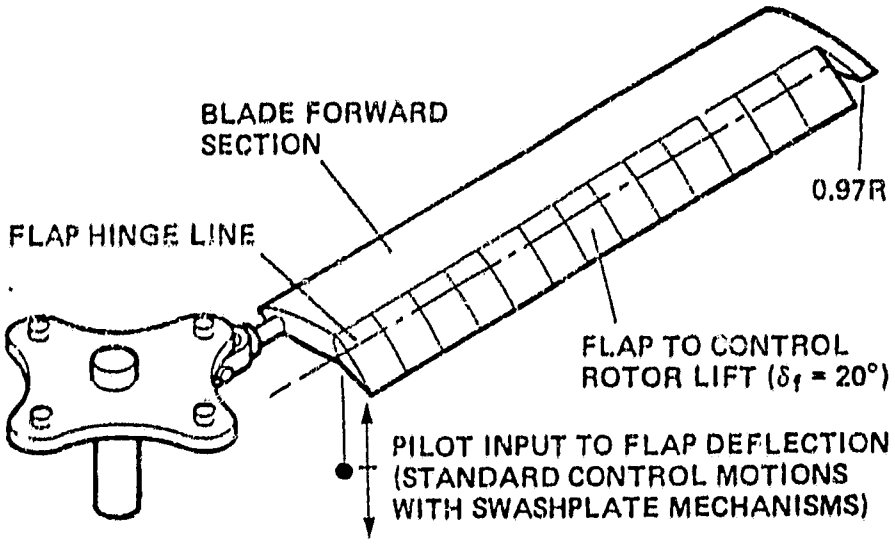

Figure 2(a). Math Model Representation of Variable Camber Rotor Blade With Trailing Edge Flaps Deflected

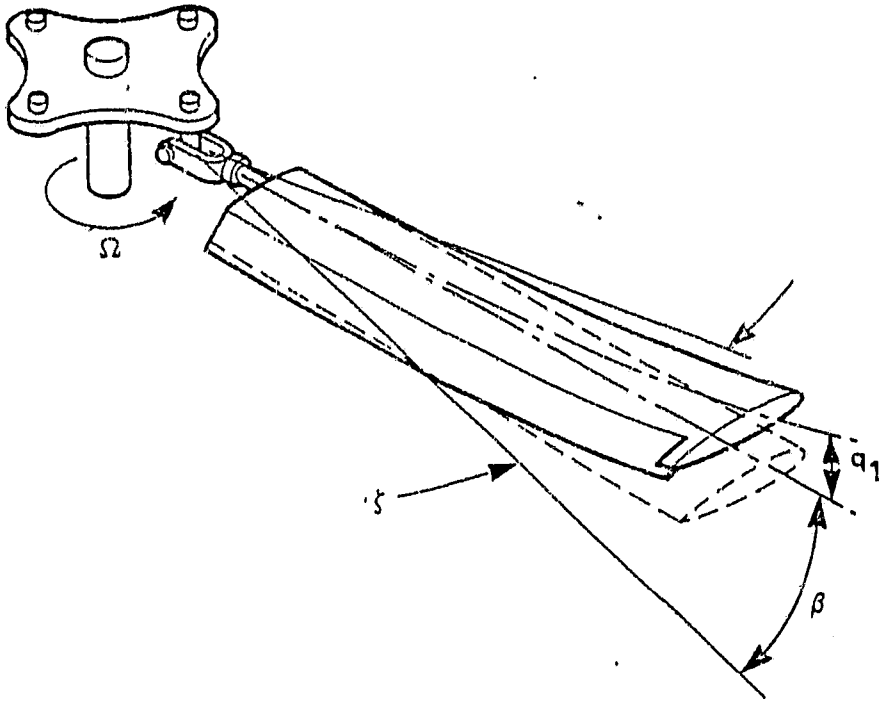

Figure 2(b). Variable Camber Rotor Blade Displacements

Figure 2. Variable Camber Rotor Blades With Falp Deflected

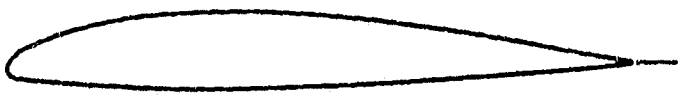

(a) FLAP NEUTRAL

(b) FLAP DEFLECTED 20°

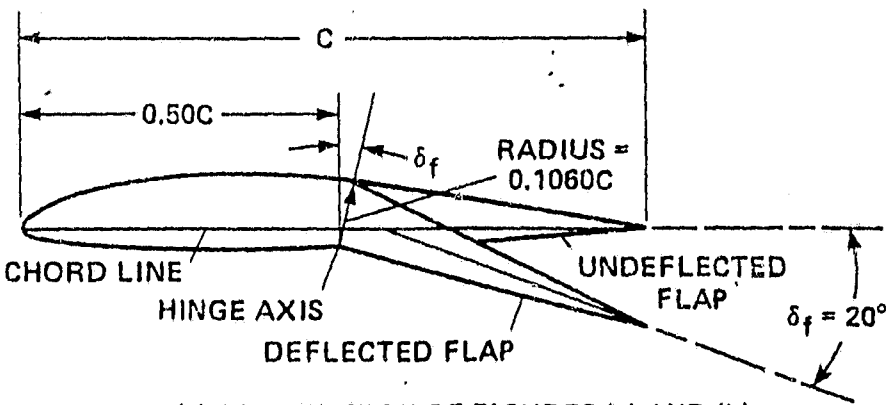

(c) COMBINATION OF FIGURES (a) AND (b)

Figure 3. Boeing Vertol VR-7 Airfoil With 0.50c Flap Deflected 20°

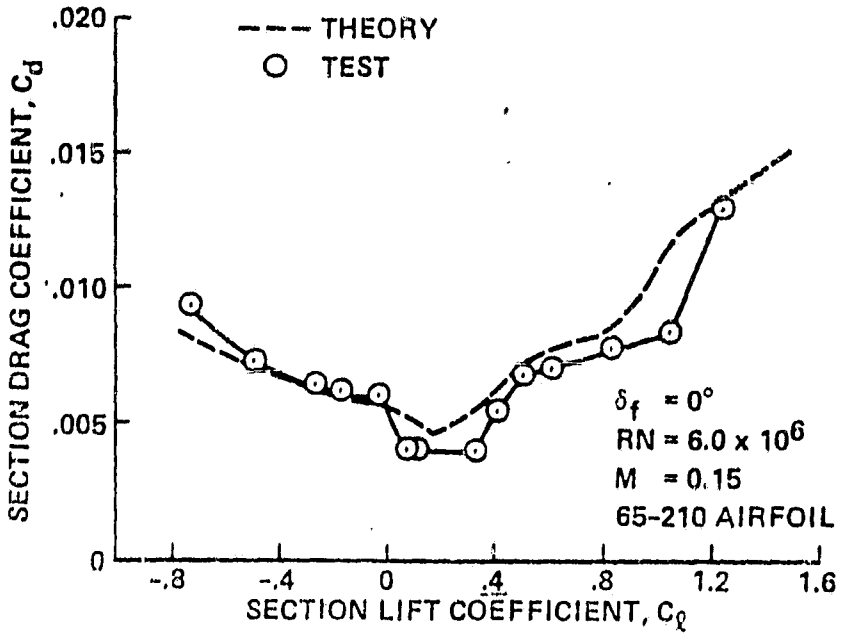

Figure 4. Test/Theory Correlation of Lift/Drag Polars for a NACA 65-210 Airfoil

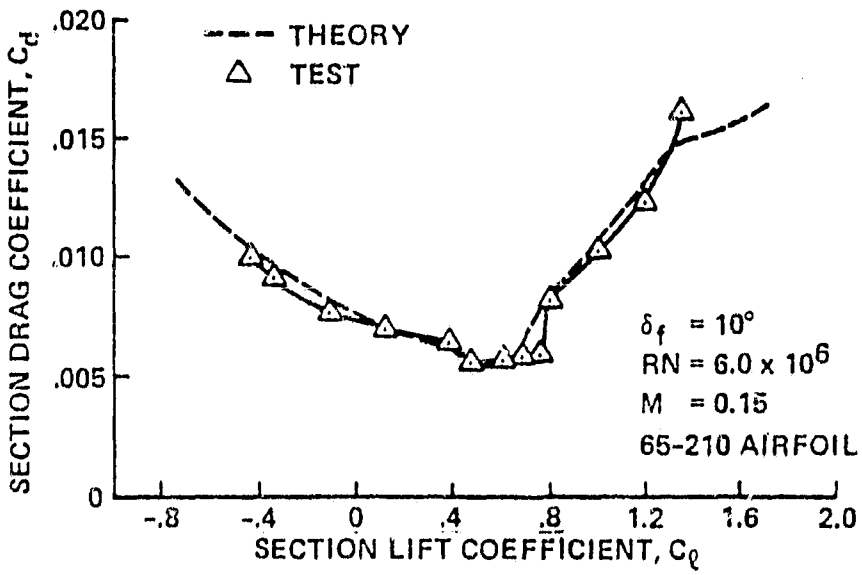

Figure 5. Test/Theory Correlation of Lift/Drag Polars for a NACA 65-210 Airfoil With a 0.50c Trailing-edge Flap

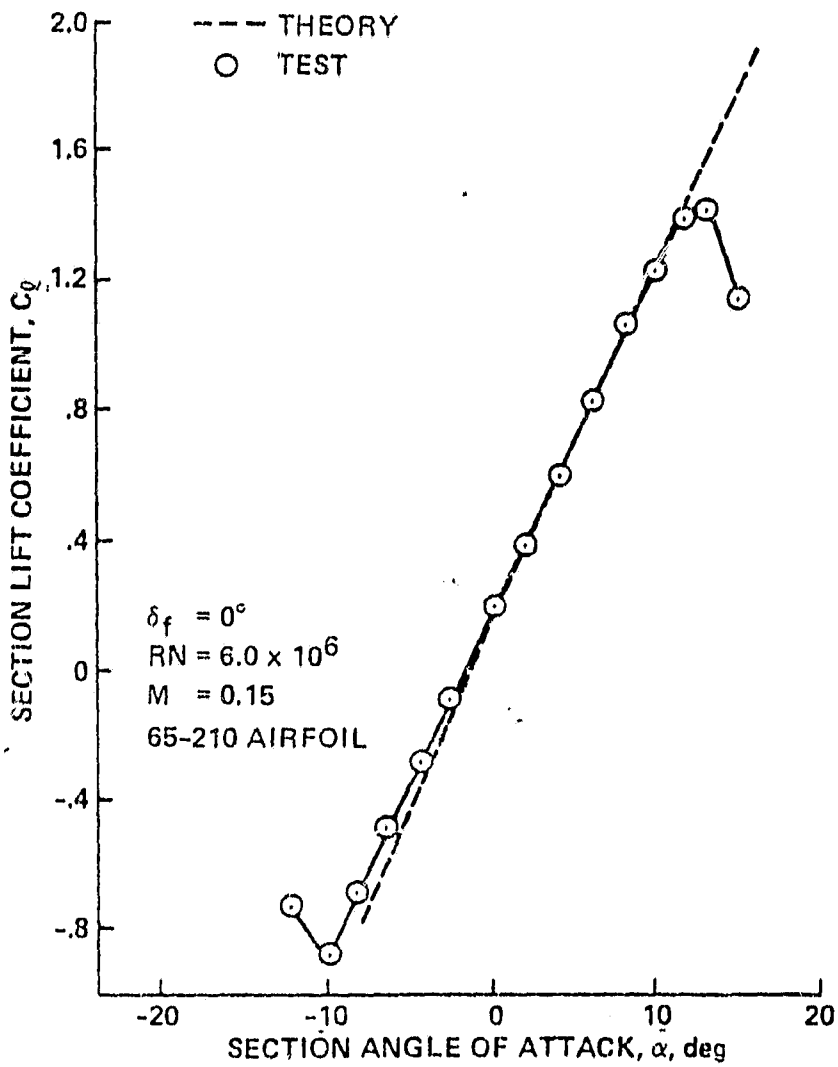

Figure 6. Test/Theory Correlation of Lift Data for a NACA 65-210 Airfoil

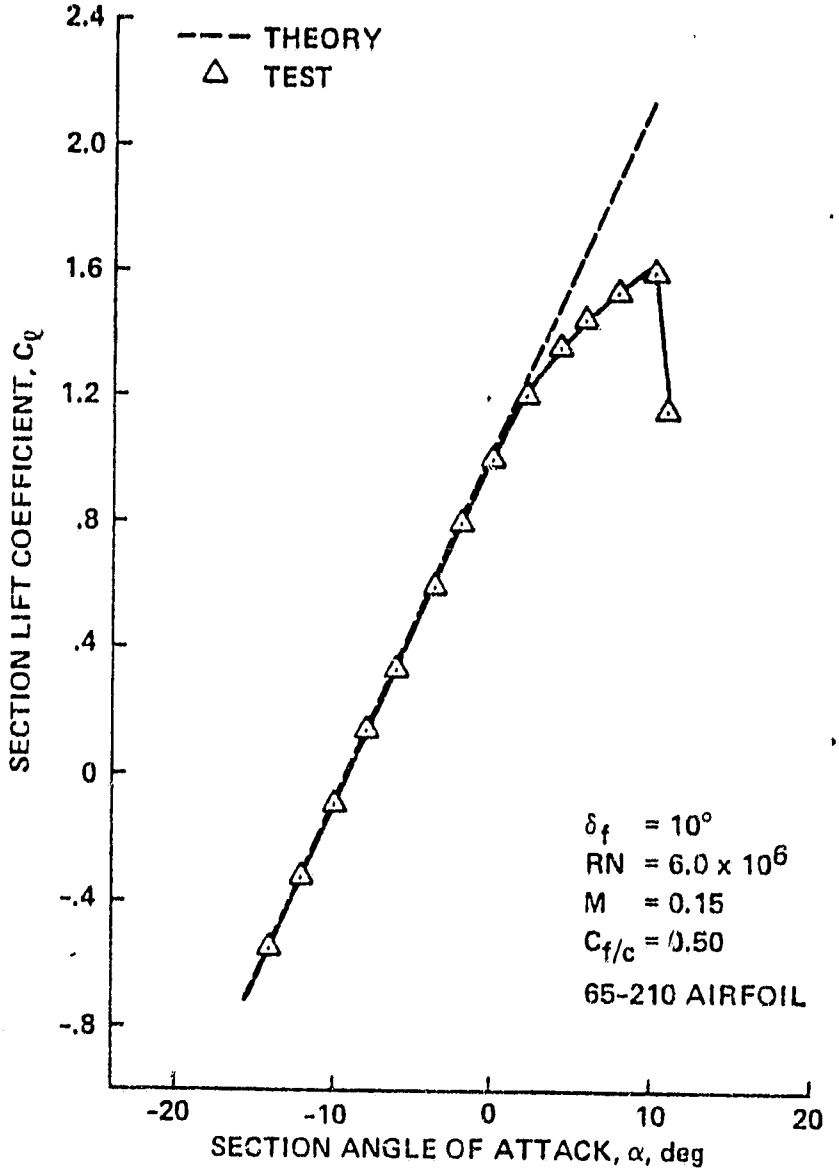

Figure 7. Test/Theory Correlation of Lift Data for a NACA 65-210 Airfoil with a Trailing-edge Flap

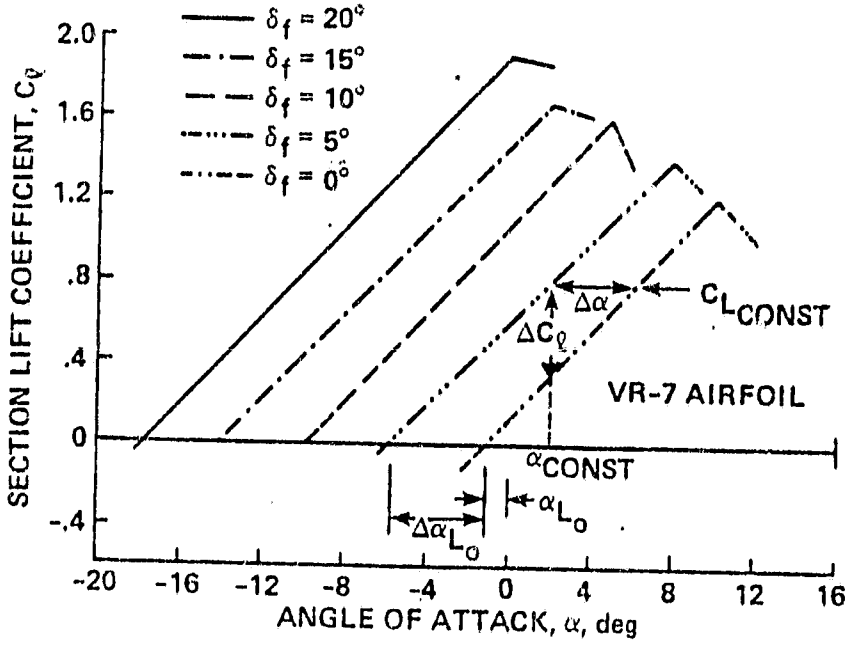

Figure 8. Numerical Analysis of the Effect of Flap Deflection on Lift Curve

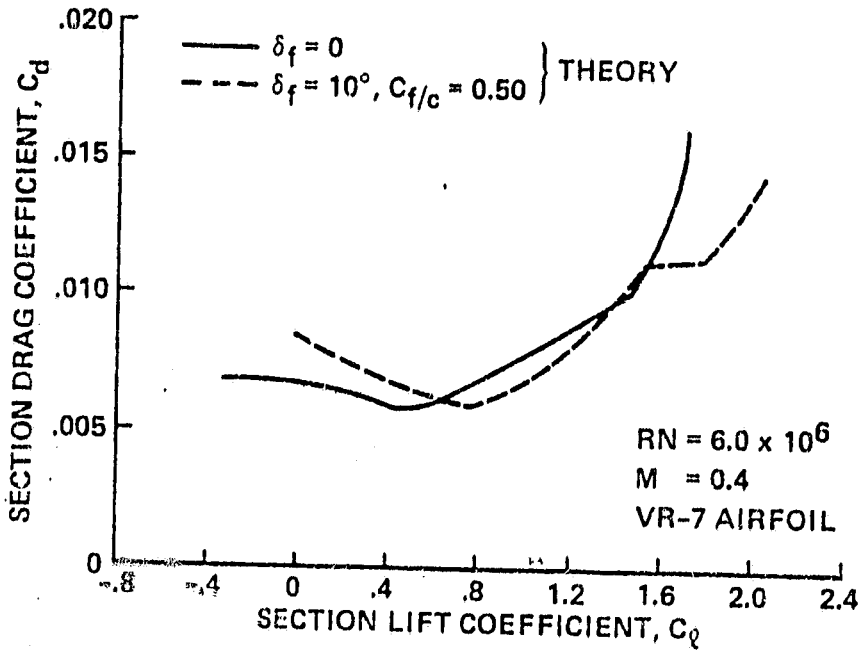

Figure 9. Lift/Drag Polars for the Boeing VR-7 Airfoil with Flap Neutral and With Flap Deflected 10°

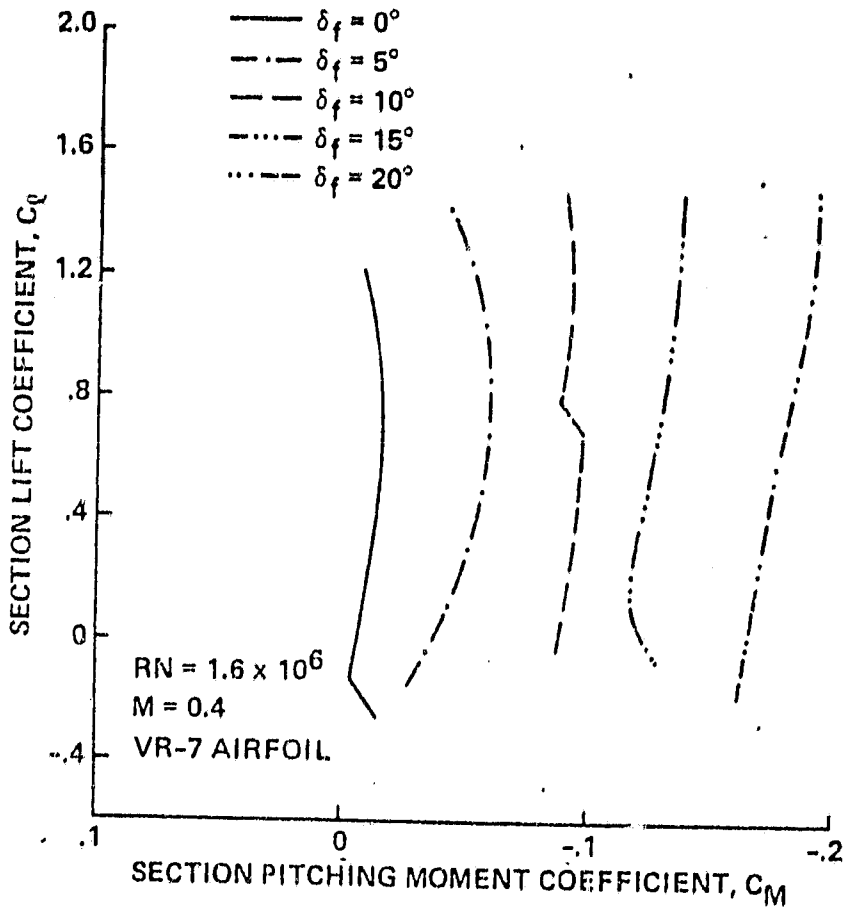

Figure 10. Numerical Analysis of Moment Data for the VR-7 Airfoil with Different Flap Deflection Angle

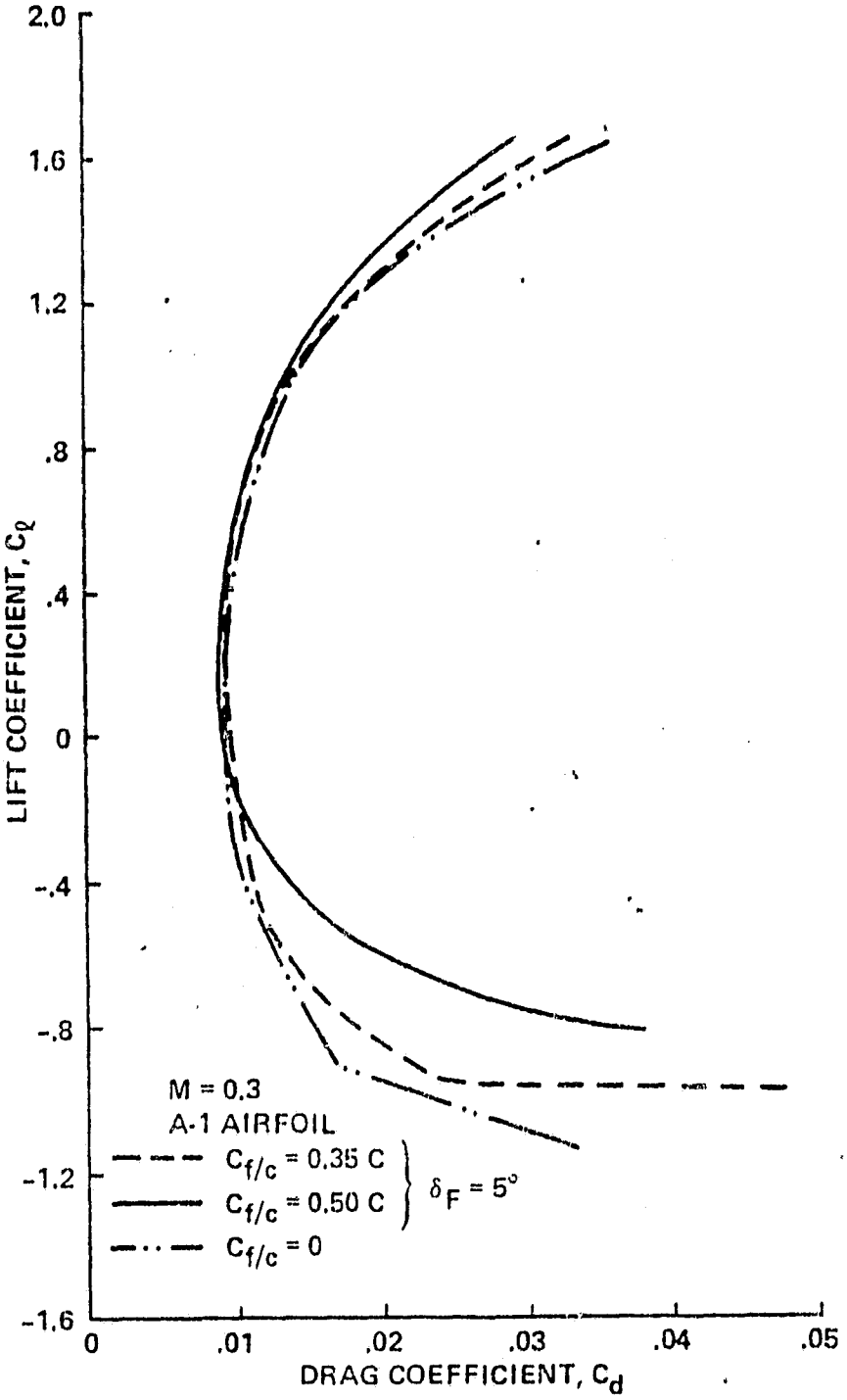

Figure 11. Lift/Drag Polars of the NASA A-1 Airfoil with Various Flap Chord Ratios

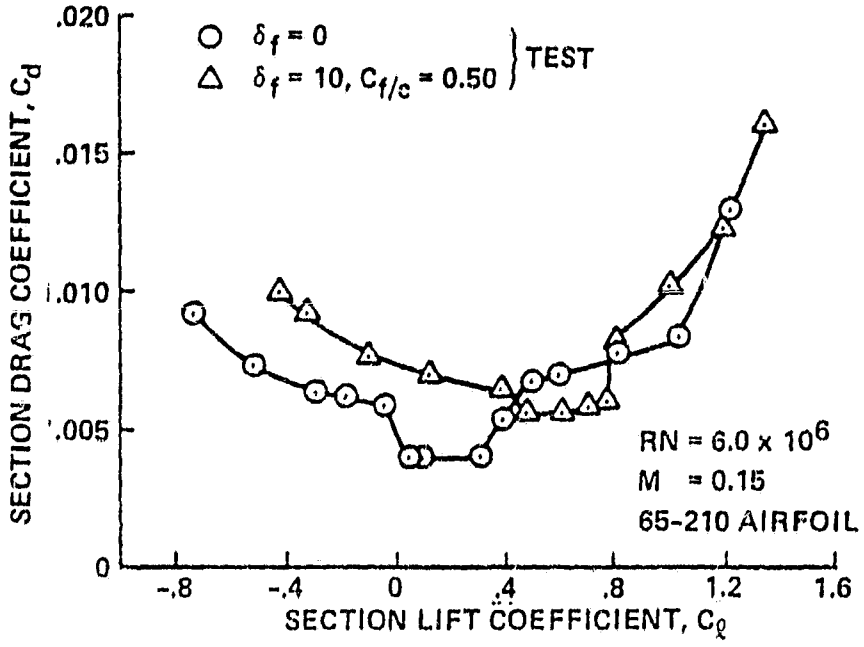

Figure 12. Lift/Drag Polars of a NACA 65-210 Airfoil for Flap Neutral and 10 Degrees Flap Deflection Respectively

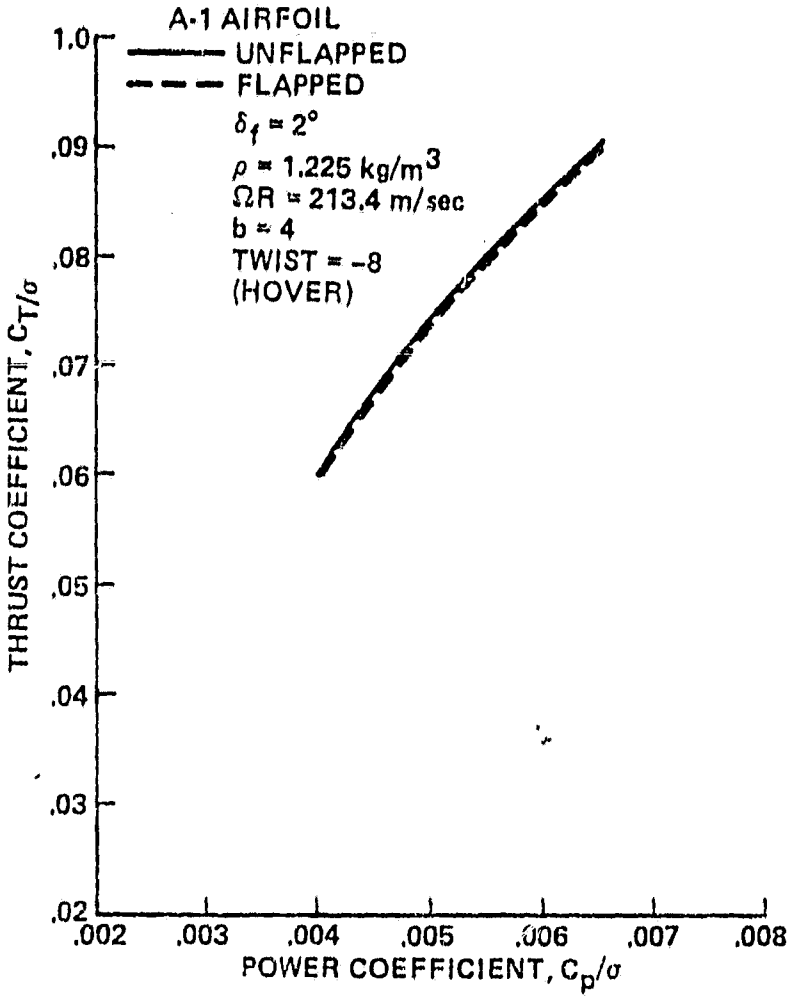

Figure 13. Numerical Analysis of Rotor Power Coefficient Versus Rotor Thrust Coefficient

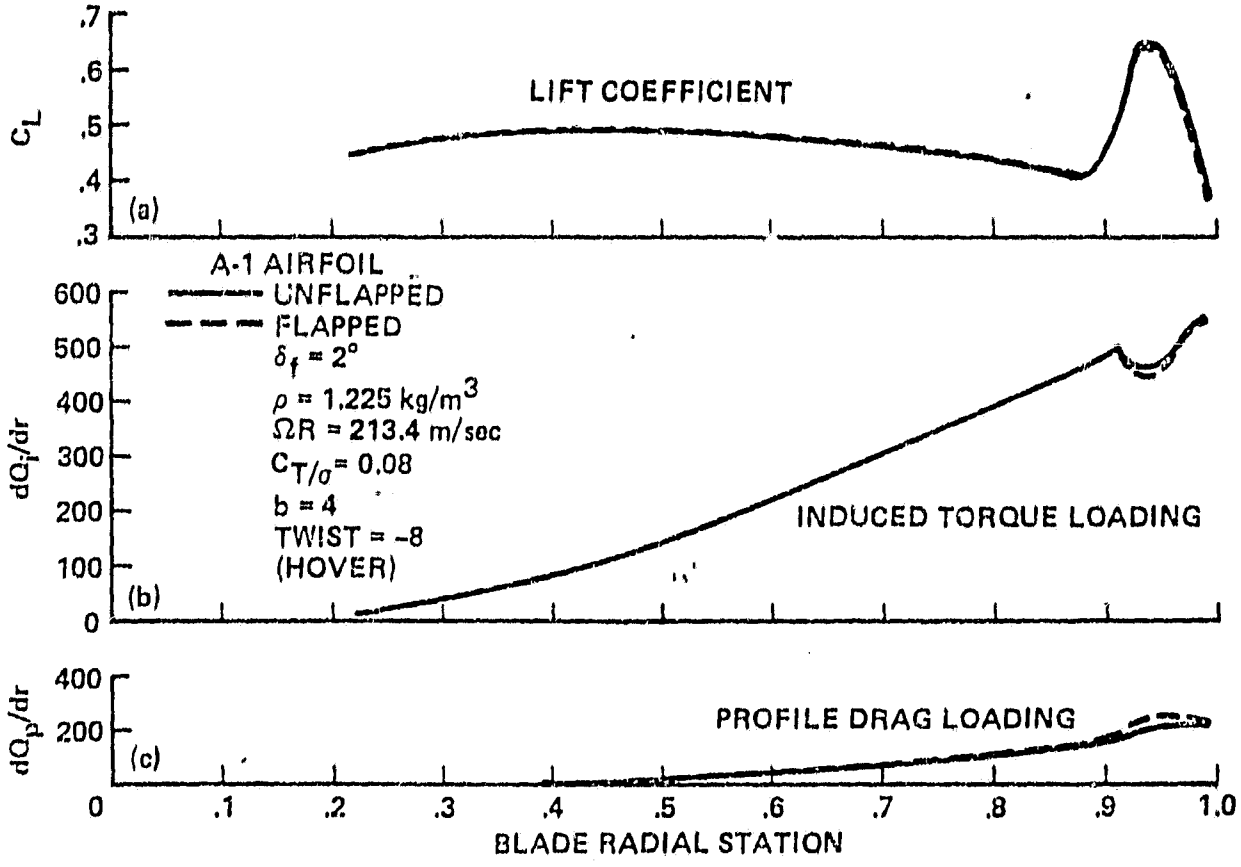

Figure 14. Numerical Analysis of Lift Coefficient, Induced Torque Loading; and Profile Drag Loading Versus Blade Radial Station

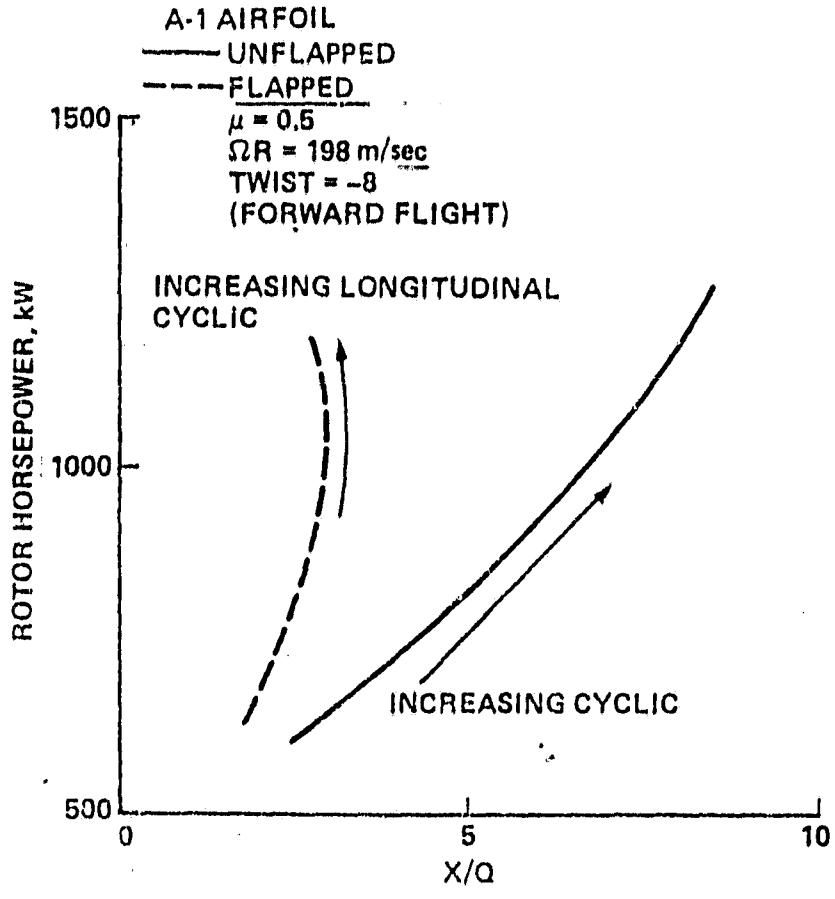

Figure 15. Rotor Horsepower Versus X/Q

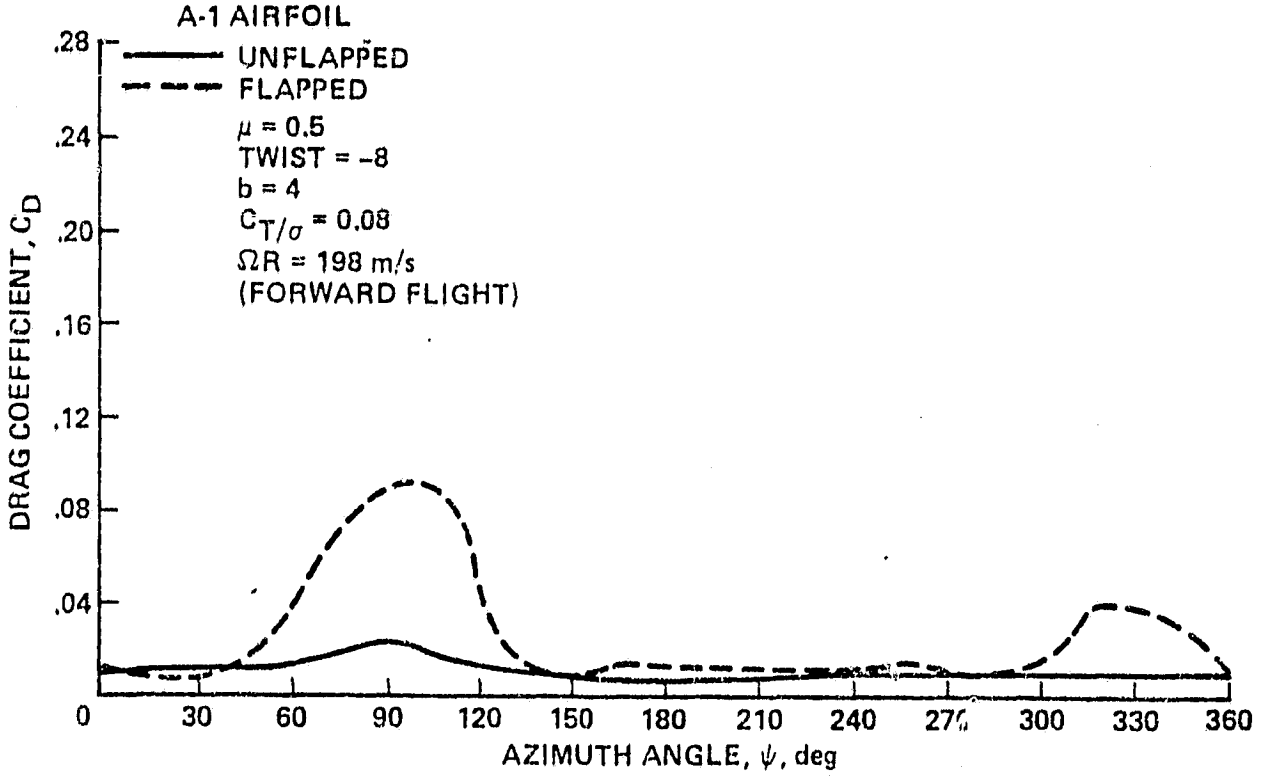

Figure 16. Drag Coefficient at the 0.968 Radial Station

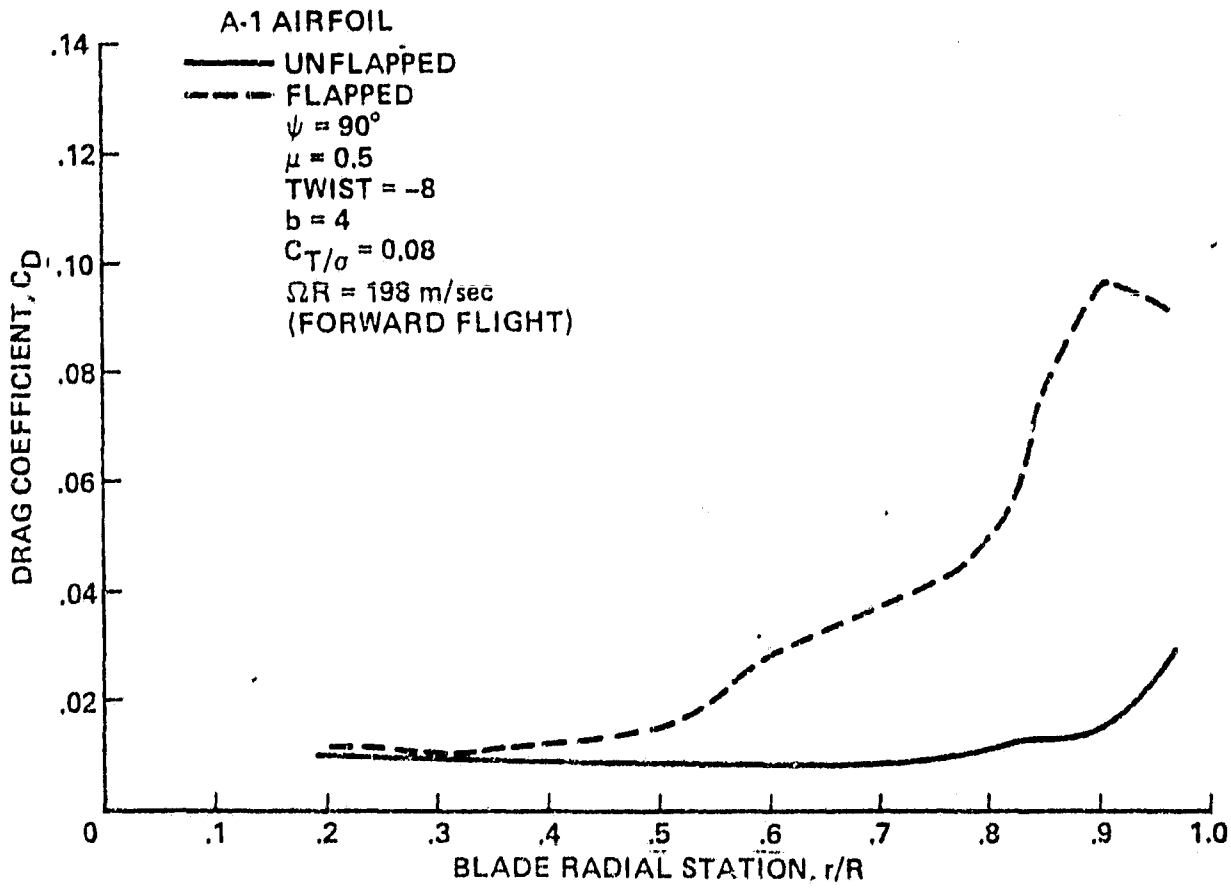

Figure 17. Drag Coefficient Versus Blade Radial Station

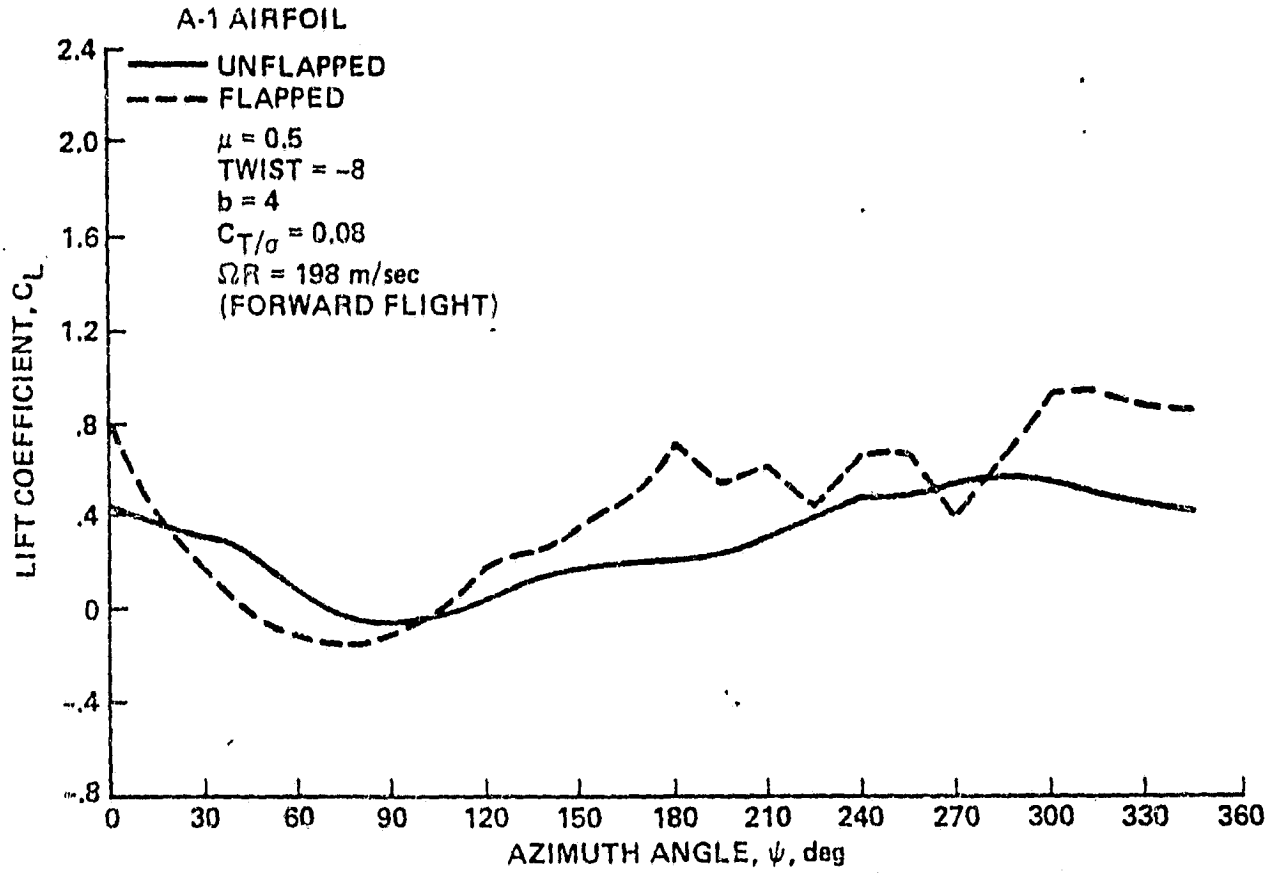

Figure 18. Lift Coefficient at the 0.968 Radial Station

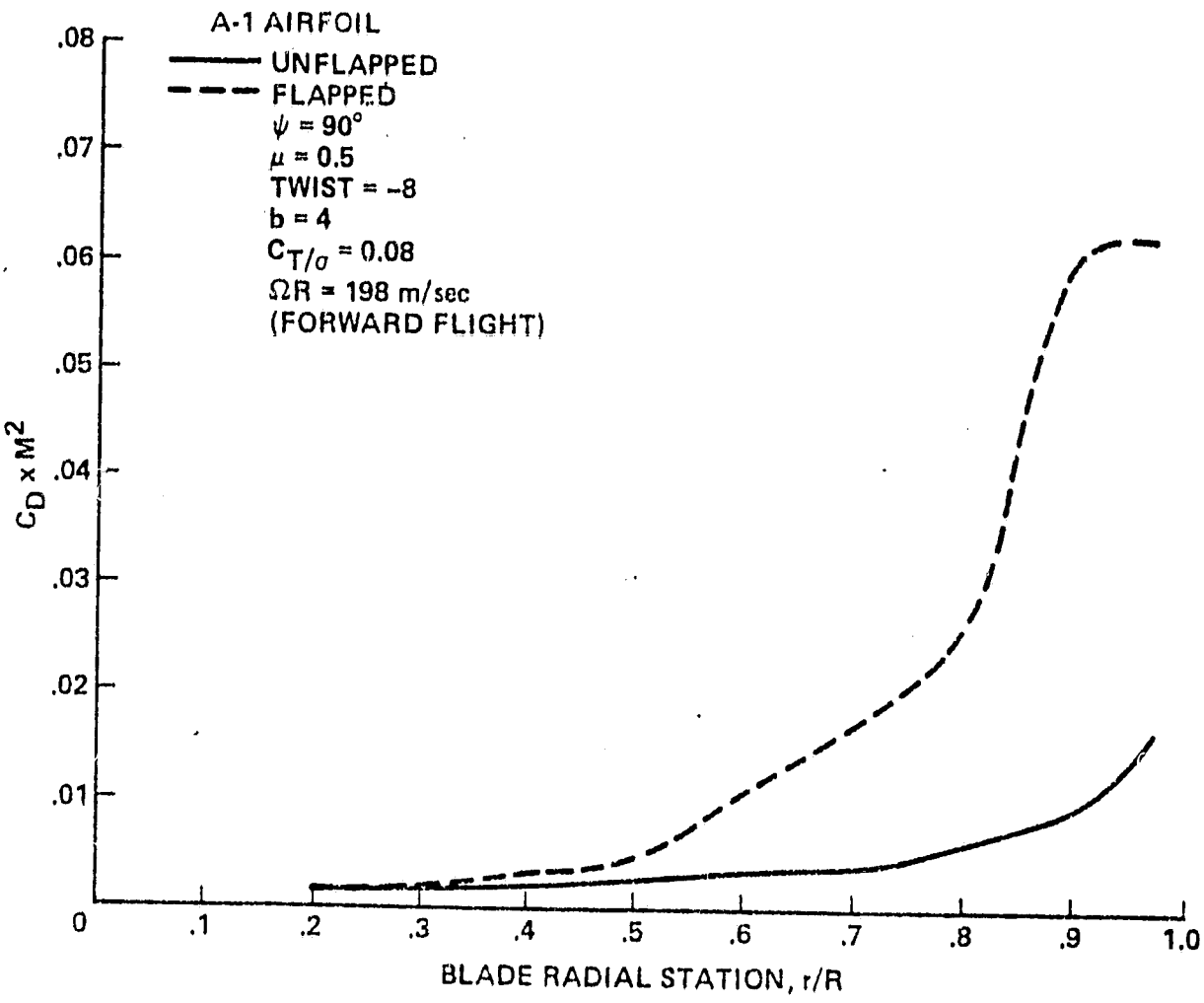

Figure 19. $C_D M^2$ Versus Blade Radial Station

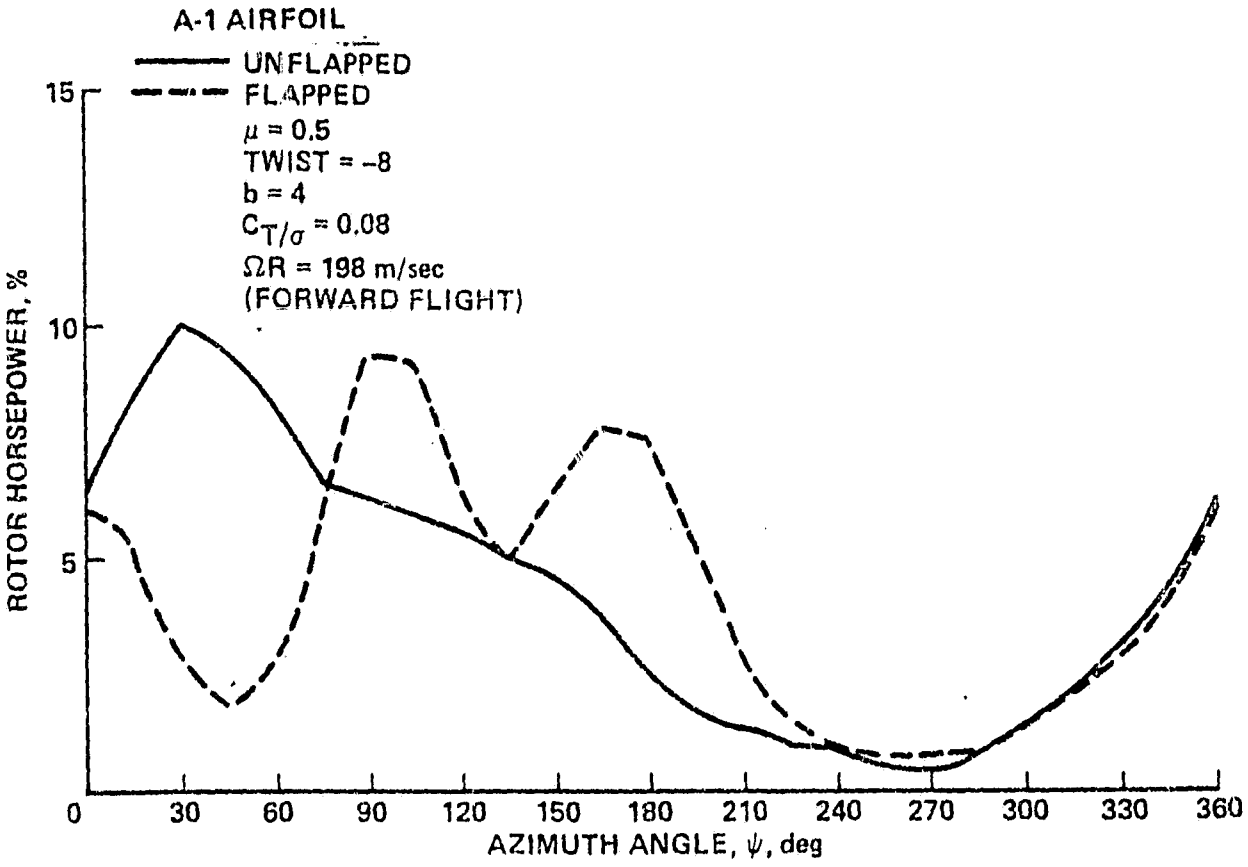

Figure 20. Rotor Horsepower (percent) Versus Azimuth Angle

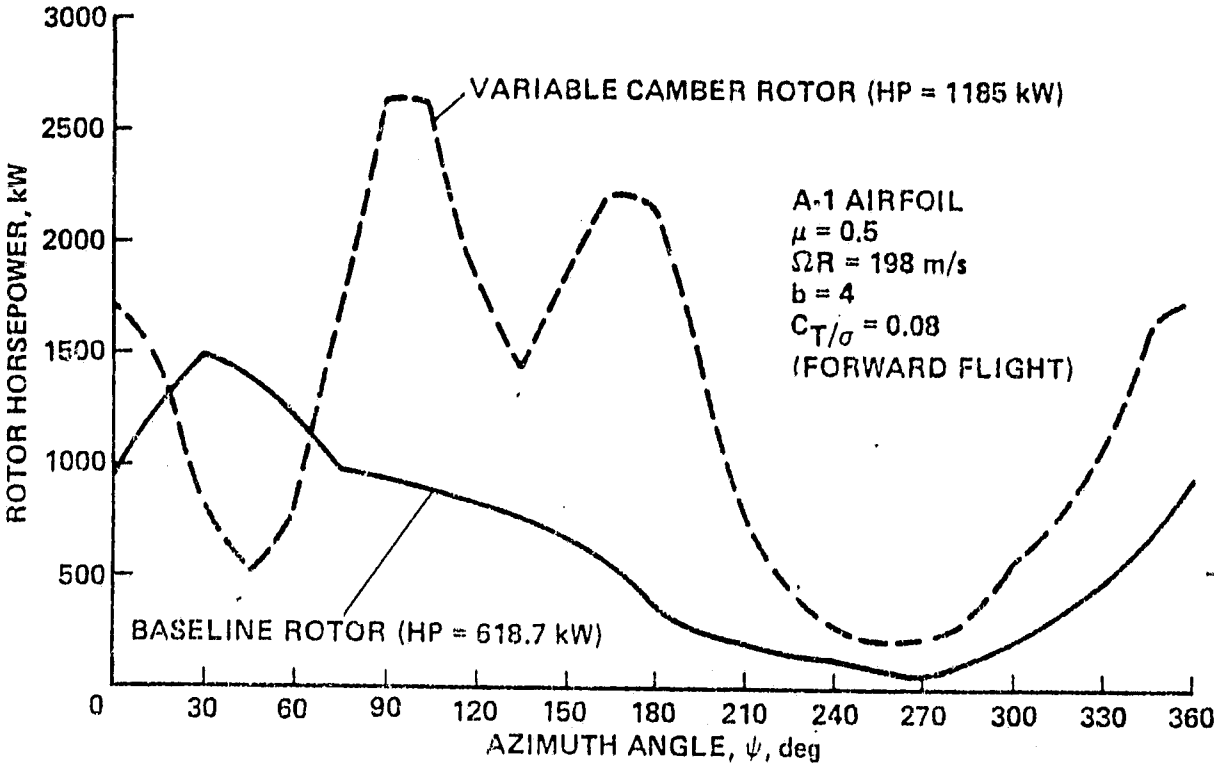

Figure 21. Rotor Power Variation at μ = 0.5

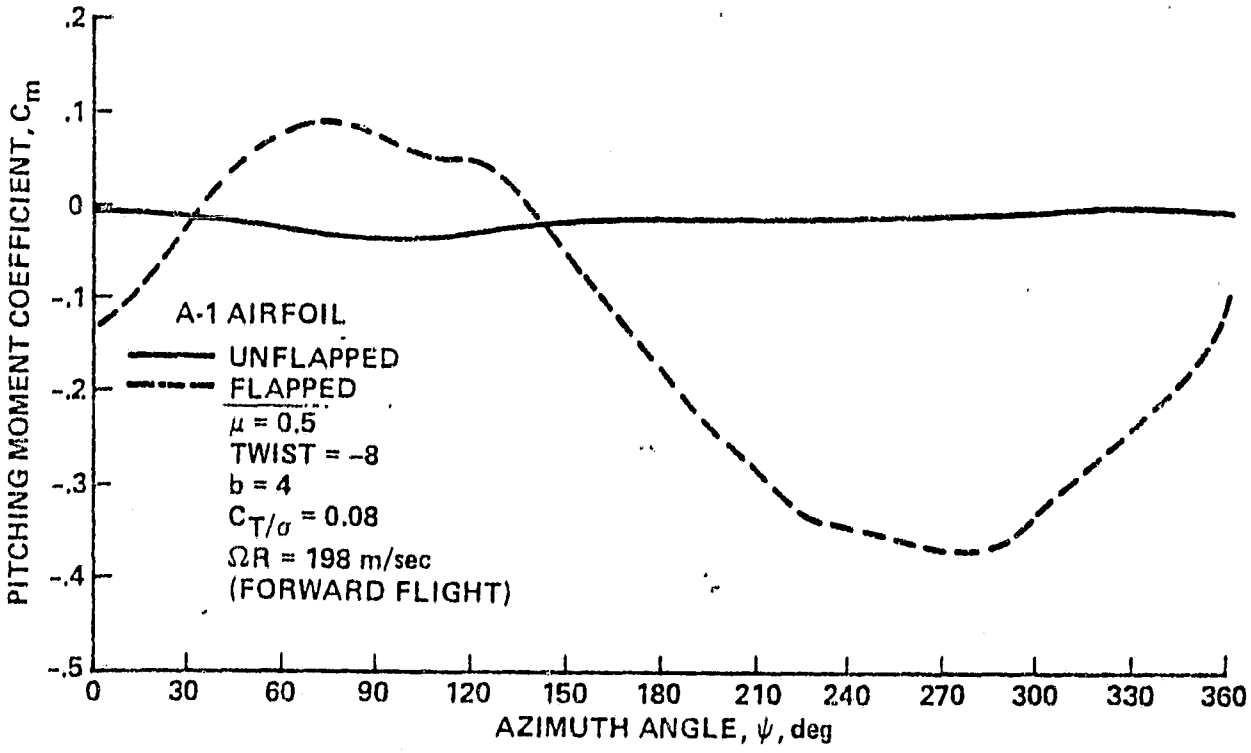

Figure 22. Pitching Moment Coefficient at the 0.968 Radial Station

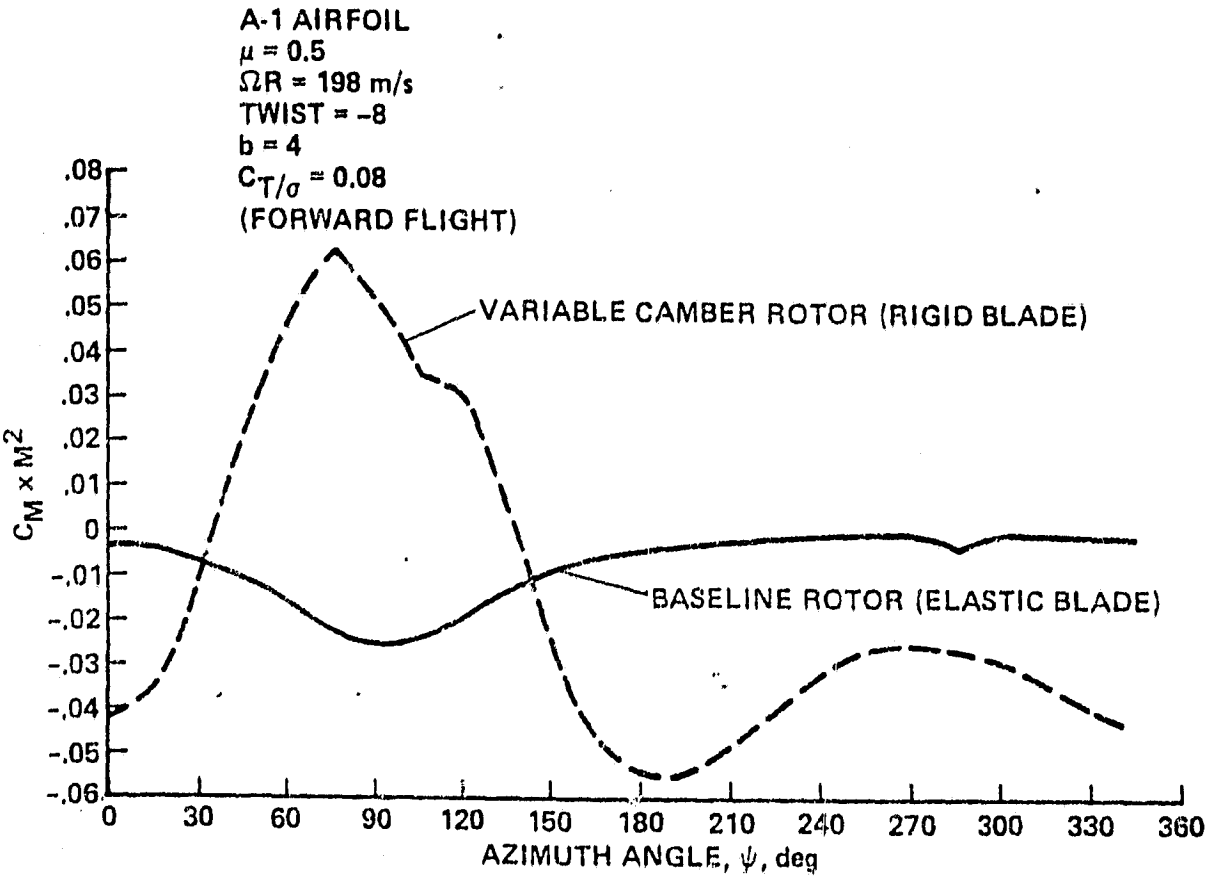

Figure 23. $C_M M^2$ Versus Azimuth Angle

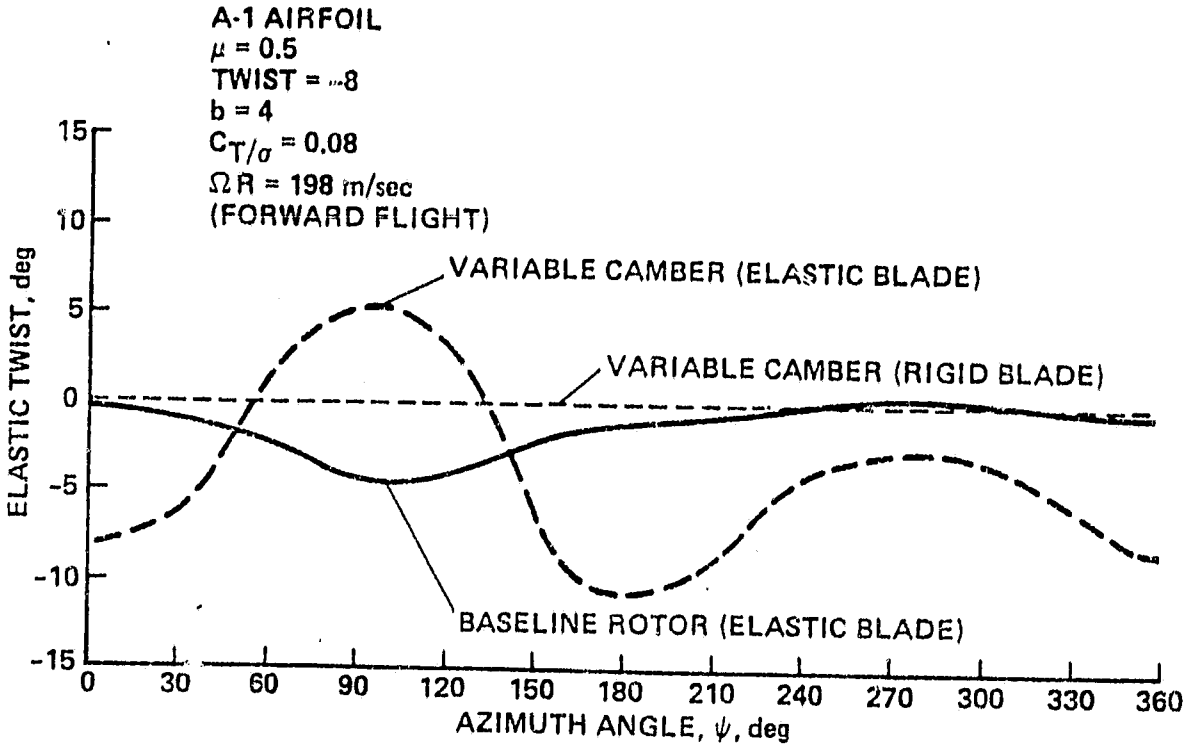

Figure 24. Blade Elastic Twist at 0.968 Radial Station